Silicon-on-Insulator Microwave Photonic Filter With Widely Tunable and Reconfigurable Flat-Top Bandpass Functionality

Claudio Porzi ⬤, Manuel Reza ⬤, Paolo Ghelfi ⬤, Marc Sorel, *Senior Member, IEEE,*
and Antonella Bogoni, *Member, IEEE*

(Invited Paper)

Abstract—We report of a silicon photonics (SiP) flat-top band-pass microwave photonic (MWP) filter with large out-of-band power rejection (OBPR) of up to more than 40 dB and exhibiting central frequency tunability over a range as large as 70 GHz, while still guaranteeing a minimum full-span OBPR larger than 25 dB. Furthermore, the RF bandpass transfer function can be widely configured without sacrificing the filter performance. In the present realization, a continuous bandwidth tuning from 5 to 10 GHz (corresponding to a 100% of bandwidth variation) is demonstrated. The operation is based on optical-to-RF mapping the response of a tunable and bandwidth reconfigurable photonic integrated optical filter, realized with a high-order distributed feedback resonator (DFBR) waveguide Bragg grating structure. A high level of functional integration is provided in a compact footprint of less than 2 mm² by embedding within the circuit a SiP phase modulator generating the modulation sideband scanning the DFBR filter, and a tunable optical splitter optimizing the MWP filter performance. Possibility of further extending system integration for monolithic on-chip operation is also investigated.

Index Terms—Microwave photonics, millimeter wave filters, optical filters, silicon photonics, waveguide Bragg gratings.

I. INTRODUCTION

INTEGRATED microwave photonic (MWP) filters have been the subject of extensive research activity in the last recent years [1], [2], [3], [4], [5], [6], [7], [8], [9], [10], [11], [12]. The

Claudio Porzi and Manuel Reza are with the TeCIP Institute, Scuola Superiore Sant'Anna, 56127 Pisa, Italy (e-mail: claudio.porzi@santannapisa.it; manuel.reza@santannapisa.it).

Paolo Ghelfi is with the PNTLab, CNIT, 56124 Pisa, Italy (e-mail: paolo.ghelfi@cnit.it).

Marc Sorel is with the TeCIP Institute, Scuola Superiore Sant'Anna, 56127 Pisa, Italy, and also with the Univerity of Glasgow, Glasgow G12 8QQ, U.K. (e-mail: Marc.Sorel@glasgow.ac.uk).

Antonella Bogoni is with the TeCIP Institute, Scuola Superiore Sant'Anna, 56127 Pisa, Italy, and also with the PNTLab, CNIT, 56124 Pisa, Italy (e-mail: antonella.bogoni@santannapisa.it).

obvious reason behind this huge amount of work originates by the need of combining the advantages brought by photonics-assisted RF signal processing with those of miniaturization. On the one hand, there are well-recognized benefits in performing analog wideband RF spectral manipulation through photonics techniques before down-conversion to IF and digital processing stages. The unique features of such photonic RF front-end processor include the vast band available and the immunity to electromagnetic interference when RF signals are up-converted to the optical domain, a large degree of flexibility in reconfiguring the system parameters (e.g., the central value and frequency extension of a bandpass microwave filter), and the possibility of remotely distributing the RF signals to be processed through a radio-over-fiber link. It is however also recognized that the reduced size, improved stability, and possibility of fabrication cost breakdown that can be attained through system integration would be the key for viable deployment of RF photonics in real-world applications [13], [14], [15].

Due to their characteristics, MWP filters are gaining new application spaces, as modern wireless communication and sensing systems keep exploring increasingly higher portions of the RF spectrum. In the evolving mobile networks scenario, broadband connectivity will be supported by using RF carriers up to the millimeter (mm-) wave region with proposed frequency bands in the $24 - 86$ GHz range [16], with maximum single channel bandwidth as wide as few GHz at 60 GHz and above [17]. In radar and sensor networks for industrial and vehicular automation, the large usable bandwidth (BW) at mm-wave frequencies translates into an improved resolution. Different applications for satellite technology also make use of a variety of frequency carriers that spans from few GHz up to the W-band (75–110 GHz) for supporting broadband user access services [18]. Antenna systems are also evolving to provide multi-band operation with demonstrated bandwidths of up to 100 GHz [19], [20]. In this context, developing integrated MWP filters for flexible selection of broadband channels would bring additional functionalities to advanced programmable RF receivers operating over multiple bands.

Yet, full on-chip MWP filter operation remains almost undemonstrated. Most of the efforts have so far concentrated on

implementing the optical core processor (e.g., a filter) in waveguide technology, while leveraging on additional bulk-optics components for complete system demonstration. For instance, RF up-conversion to the optical domain is typically performed using external electro-optic (EO) modulators, either because the performance of photonic integrated devices is not yet as mature as that of commercial devices, or because high-speed EO effect is not supported by the platform providing the high-performing integrated optical filter processor. In [2] and [7], the BW reconfigurability of MWP filters based on photonic integrated frequency comb sources, has been realized through expensive equipment in liquid-crystal-on-silicon (LCoS) technology, which hinders cost-effective device utilization in practical system applications. Frequency tuning and BW reconfiguarability of a bandpass optical filter (OF) realized in InP technology has been demonstrated in [1]. The integrated OF has been employed to realize a programmable MWP filter using an off-chip EO modulator, but reduction in the optical/microwave filters rejection is observed as the passband width is changed. A monolithic silicon-on-insulator (SOI) photonic integrated circuit (PIC) has been reported in [5] to realize a tunable integrated MWP bandpass filter. Both on-chip up- and down-conversion to/from the optical domain are provided for the input and output RF signals, respectively, using silicon photonics (SiP) phase modulator (PM) and photodiode (PD), with an intermediate OF processing stage. Despite the demonstrated full on-chip functionality, the performance of the MWP filter are limited by a non-flat and shallow-roll-off passband frequency response, a restricted tuning range of ∼10 GHz, and a strong dependence of the filter features on the the tuning frequency. A similar trade-off between functional integration level and system performance is observed in [3], where limited tunability, roll-off, and rejection of the monolithic InP-based MWP filter is also noticed. A hybrid-packaged MWP filter, where a silicon chip comprising modulator, high Q-factor filter, and photodetector is coupled to an InP DFB laser die through micro-optics components has recently been presented [11]. Also in this case, the obtained RF response is limited in terms of passband flatness and roll-off, with a maximum rejection of about 15 dB over a tuning range restricted to 20 GHz.

Here, we report of a SOI MWP filter realizing flat-top bandpass functionality with abrupt roll-off and large rejection of up to more than 40 dB. On-chip optical up-conversion and processing through a high performance OF and a tunable actuator is provided for the input RF signal. A tuning range over 70 GHz with only moderate degradation of the rejection capability when centering for filter centered above about 50 GHz is demonstrated. Additionally, the BW of the filter can be continuously varied without affecting its performance. BW tuning from ∼5 to 10 GHz is observed with this preliminary circuit realization. Although wideband filters are of interest for band pre-selection in mm-wave receivers for high data-rate wireless communications or for wideband radar systems operating over multiple bands [21], [22], [23], smaller BW values can be tailored in future designs for further extending the application range of the circuit.
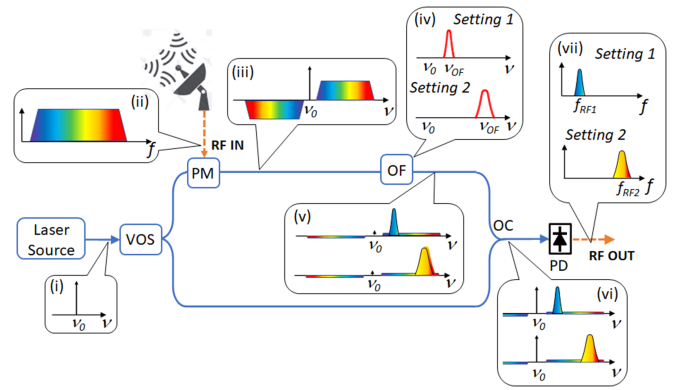

Fig. 1. Schematic operation of the proposed tunable and bandwidth reconfigurable microwave photonic bandpass filter (VOS: variable optical splitter; PM: phase modulator; OF: optical filter; OC: optical coupler; PD: photodiode).

II. INTEGRATED MWP FILTER OPERATION AND PIC REALIZATION

The proposed integrated MWP filter simply exploits the optical-to-RF mapping of a bandpass OF when scanned by the modulation sideband of an EO modulator [24], [25]. The OF response can then be reconstructed in the RF domain through the beating within a PD between the sampling sideband and the original optical carrier. To produce the beating tone with this technique, either both the carrier and the sideband are let through the filter, which allows for realizing only low-pass characteristics of the MWP filter [3], or solely the scanning sideband falls within the OF band before being recombined with the optical carrier [26], [27]. In this last approach, a bandpass MWP filter with central frequency defined by the detuning between the laser carrier and the OF can be realized. Furthermore, the possibility of changing by some means the OF BW would directly reflect into the width of the high-transmission region in the MWP filter transfer function [1]. The schematic operation for such tunable and BW reconfigurable MWP filter is then illustrated in Fig. 1.

In the scheme, the output light from a laser source (LS) at the optical frequency ν_0 (i) is sent to a variable optical splitter (VOS), where it is separated into two paths. On the upper path in the figure, a PM up-converts to the optical domain the broadband RF signal from a receiving antenna (ii). The overall driving power is assumed to be sufficiently below the modulator half-wave voltage, so that only the first-order sideband replica of the RF spectrum can be considered at positive and negative frequencies around ν_0 (iii). At the output of the PM, a bandpass OF with central frequency ν_{OF} properly detuned from ν_0 (iv) selects a portion of either the upper or lower sideband, while strongly suppressing all the other spectral components (v). Two possible settings for the bandpass OF, involving the tuning of both its BW and central frequency are illustrated in the example. After the OF, the selected portion of the optical spectrum is recombined through an optical coupler (OC) with the laser carrier emerging from the other branch of the VOS (vi). The composite signal at the output of the OC is then routed to a PD that down-converts back to the RF domain the selected portion
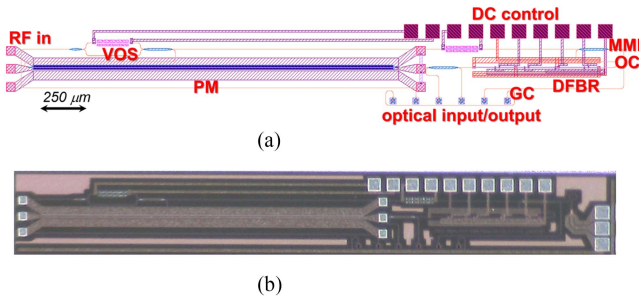
Fig. 2. (a) Mask layout for circuit implementation in silicon-on-insulator technology (DFBR: distributed feedback resonator; MMI OC: multimode interference optical coupler; GC: grating coupler). (b) Micrograph of the fabricated photonic integrated circuit.

in the sideband spectrum corresponding to a given setting of the OF (vii). By acting on the VOS, the relative amplitude between the re-inserted carrier and the scanning sideband impinging on the PD can be finely adjusted, which allows the optimization of the integrated MWP filter performance.

The circuit has then been realized in SOI technology, and the produced mask layout for device fabrication using standard DUV lithography through a multi-project wafer service [28] is shown in Fig. 2(a). The PM is a 2-mm-long carrier-depletion-based device, and the integrated OF is implemented in a high-order multi-cavity distributed feedback resonator (DFBR) architecture [29]. The VOS is realized using a symmetric balanced Mach Zehnder interferometer (MZI) with thermal phase control onto its arms. The output OC is implemented with a 2×2 multi-mode interference (MMI) device, with one output connected to the PIC optical output port for subsequent down-conversion to RF domain of the OSSB modulated signal through an external high-speed PD. A replica of the PIC output optical signal is also delivered to a test on-chip SiP Ge PD. Grating couplers (GCs) provide access to the optical input/output ports through a fiber array, and metal routes and pads are used for contacting the heaters controlling the DFBR filter and the VOS. An additional 2×2 MMI splitter is also inserted between the DFBR and PM for the purpose of monitoring both the filter transfer function and the modulator spectrum. Thanks to the minimized modulator complexity and to the compact layout of the narrow-band photonic integrated DFBR filter, the circuit exhibits a small footprint with an overall on-chip occupied area of ~ 1.8 mm^2, including metal routes and pads. A microscope image of the fabricated PIC is also shown in Fig. 2(b).

III. PIC CHARACTERIZATION

The operation of the main functional elements of the PIC, i.e., the SiP DFBR filter and the PM, is reported in the following, illustrating their role for realizing the broadly tunable and reconfigurable functionalities of the integrated MWP filter.

A. Tunable and BW Reconfigurable Photonic Integrated OF

In this paragraph, the DFBR OF architecture, which is the core element of the scheme, is described and the results of its experimental characterization are presented. Compared to

other photonic-integrated filtering approaches, such as coupled microring resonators (MRRs), DFBRs can simplify the design of narrow bandpass transfer functions down to the GHz-range within large bandstop regions [29], as required for processing wideband RF signals. Additionally, grating-based devices provide an ultra-compact wire-like filter geometry.

An illustrative representation of the filter structure is shown in Fig. 3(a), whereas the detailed view of the actual mask layout is reported in Fig. 3(b). The structure realizes a 4th-order multi-cavity filter by embedding four phase shift (PS) sections between five BG mirrors (BGMs) realized in a laterally-corrugated silicon strip waveguide. By choosing the proper number of periods for the BGMs, a passband window within a bandstop region defined by the BW of the mirrors can be shaped in the filter spectral transmission [30], [31]. Since the resonances of the coupled cavities are sensitive to fabrication imperfections, local micro-heaters (MHs) are used to control the optical path of each PS section [32]. In this realization, the MHs are implemented with a pair of doped silicon resistors that are connected in parallel and symmetrically placed at 1 μm from the sidewalls of the PS sections. A top metal long heater (LH), covering the whole length of the structure, is additionally deposited above the oxide cladding in correspondence of the waveguide. As shown in the DFBR mask layout, two different metal layers are used to realize the different connections between the various MH and LH signals and ground electrodes. As also shown, the fabricated LH is segmented into four sections connected in parallel to optimize its resistance. Besides allowing compensation of the scattering of the resonances originated by the unideal lithographic process, the MHs also provide an effective mechanism for tuning the passband window within the bandstop region without affecting its edges [32]. On the other hand, the role of the LH is to perform a rigid translation of the whole stopband, changing *de facto* the Bragg wavelength, λ_b, of the grating mirrors by increasing the optical length of the corrugation period through thermo-optic effect. These two tuning mechanisms allow the OF central frequency and BW to be independently controlled, as explained in the following. When the optical path of the PS sections matches an odd multiple of $\lambda_b/4$ (i.e., half the corrugation period), the passband peak lies in the center of the stopband. In this case, the highest possible Q-factor is attained for the coupled cavities, since the BGMs reflectivity is maximum at around λ_b. As the resonant wavelength of the filter is shifted toward the edges of the stopband, the Q-factor of the cavities decreases, due to the roll-off of the grating strength away from λ_b [33]. Consequently, the BW of the passband gets larger. To enhance this effect, and facilitate the filter reconfigurability at moderate power levels of the MHs, the DFBR has been realized such to provide a relatively narrow stopband width and adopting a long-cavity design, in which the PS sections are nominally set to be 101 times longer than the typical quarter-wave value of phase-shifted BGs.

The measured spectral transmission of the fabricated DFBR filter and the details of the passband window when the MHs are set such that the transmission peak lies close to middle of the stopband are reported in Fig. 4(a) and (b), respectively. A -3 dB BW of 4.5 GHz is measured for this case, with a sharp
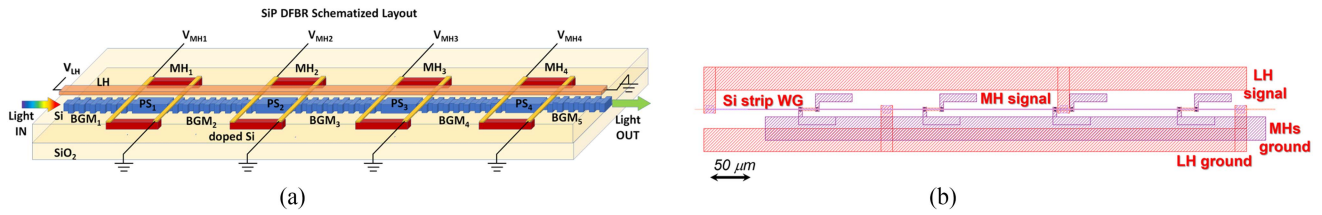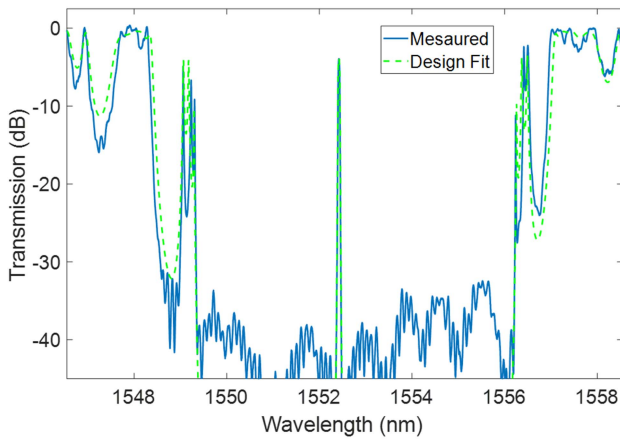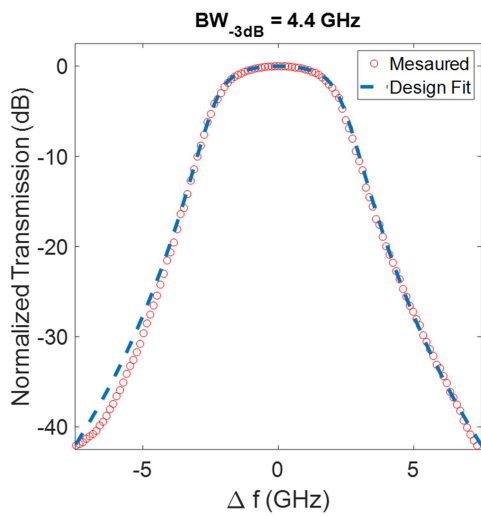
Fig. 3. (a) Artistic representation of the silicon photonics (SiP) distributed feedback resonator (DFBR) filter (BGM: Bragg grating mirror; PS: phase shift; MH: micro-heater; LH: long heater). (b) Details of the DFBR mask layout.
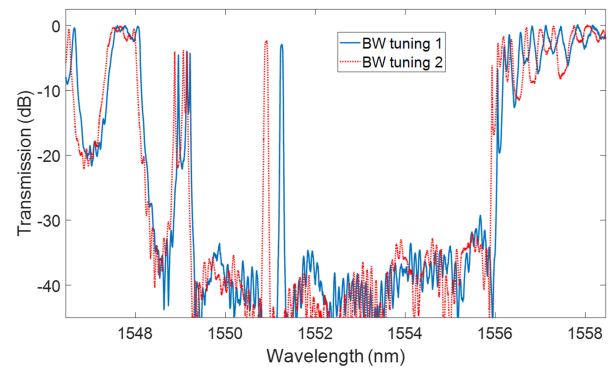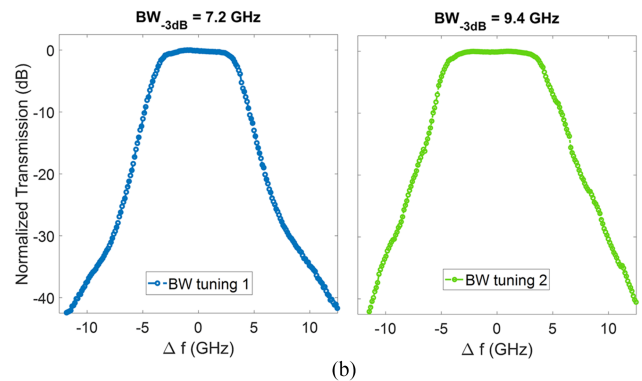

Fig. 5. (a) Two different passband tuning within the DFBR stopband, leading to two different values of the filter bandwidth (BW). (b) Corresponding details of the passband windows.

Fig. 4. (a) DFBR spectral reflectivity for passband window tuned in proximity of the Bragg wavelength. (b) Details of the passband window.

In Fig. 5(a), two different passband positions closer to the shorter wavelength edge of the stopband with respect to Fig. 4 are shown. The corresponding details of the filter transfer functions around the transmission peak are then reported in Fig. 5(b), illustrating that a BW value of 7.2 and 9.4 GHz is observed when the passband central frequency is spaced away from the the stopband center (i.e., the Bragg wavelength), by about 2 and 2.4 nm, respectively. Finally, by applying a tuning signal to the LH control electrode, the central frequency of the reconfigured bandpass transfer function can be changed over ranges as wide as few nanometers [35], [36], [37], allowing for separate control of the filter BW and central wavelength. As an example, the observed DFBR transmission spectra when the passband window is tuned in the middle of the stopband at two different voltage signal levels applied to the the top metal LH, for a wavelength shift of the fixed-bandwidth passabnad of ∼1.8 nm, is shown in Fig. 6.

roll-off leading to a rejection of more than 28 dB at a detuning of 5 GHz from the center of the flat-top region. For this DFBR realization, the measured filter BW at the stopband center is larger than the target design value of 2 GHz. However, all the relevant parameters for the fabricated grating can be extracted through numerical fitting of the experimental traces (also shown in the figures), permitting to calibrate future designs with this specific fabrication process [34].
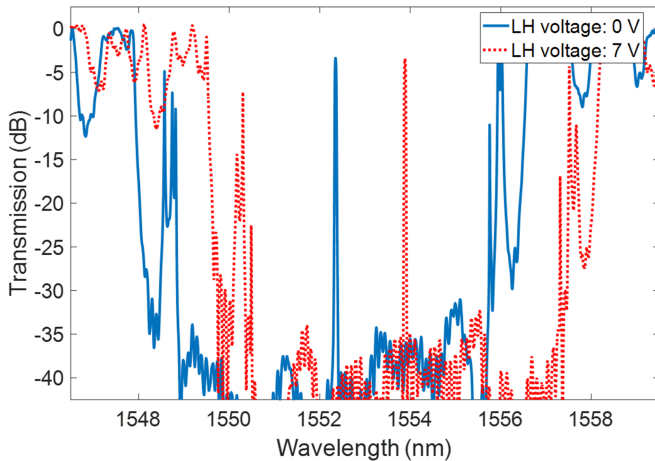
Fig. 6. Fixed-bandwidth passband central wavelength tuning by applying different voltage levels to the top metal long heater (LH) of the silicon photonics distributed feedback resonator structure.
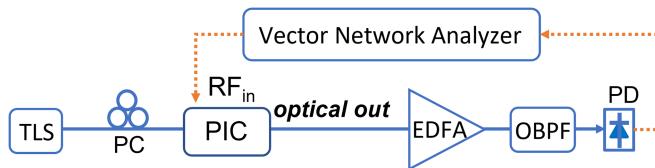

Fig. 7. Experimental setup for characterizing the silicon-photonics phase modulator and integrated MWP filter (TLS: tunable laser source; PC: polarization controller; PIC: photonic integrated circuit; EDFA: erbium-doped fiber amplifier; OBPF: optical bandpass filter; PD: photodiode.

B. SiP PM Characterization

The small-signal modulation BW of the SiP PM is then characterized using the setup of Fig. 7. A 67-GHz BW vector network analyzer (VNA) sweeps the modulator driving frequency at the RF input port of the PIC in the range between 10 MHz and 70 GHz and collects the signal detected by a 70 GHz-BW external PD which is connected to the optical output port of the PIC. A bias tee (not shown in the figure) is employed to provide the DC reverse bias for the modulator pn-junction. A polarization controller (PC) is used to maximize the injected optical power into the circuit from a tunable LS (TLS) through the input GC. An erbium-doped fiber amplifier (EDFA) at the PIC output, followed by an optical bandpass filter (OBPF), raises the signal level at the PD input to about 3 dBm. In the measurements, the output wavelength from the TLS is matched to the central frequency of the DFBR filter passband window. The optical power entering the circuit is then evenly split onto the two output branches of the VOS, thus making the scheme of Fig. 1 acting as a MZI, which is then biased at quadrature using a thermally controlled optical phase shifter (OPS) placed on the carrier path (see Fig. 3(a)). The measured normalized squared magnitude of the S_{21} parameters from the VNA for different reverse bias values of the modulator pn-junction are shown in Fig. 8. A calibration trace obtained after bypassing the PIC is subtracted to all the mesaurements to eliminate the frequency response of the bias tee and RF cables. Although the measured maximum 3 dB cut-off modulation frequency of the
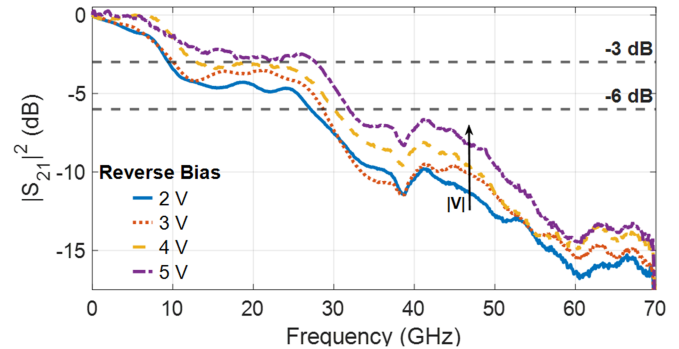

Fig. 8. Measured carrier-depletion-based phase modulator small-signal response under different reverse-bias voltage conditions.

device stays below 30 GHz under any bias condition, a slow roll-off of the small-signal response down to about 15 dB below the low-frequency value is observed at the maximum driving frequency of 70 GHz.

IV. INTEGRATED MWP FILTER RESULTS

The various performance parameters, including the tuning and reconfigurability features of the integrated MWP filter, are then assessed using the same setup of Fig. 7 under different experimental conditions. The effect of tuning the VOS on the filter RF gain and spurious-signal rejection capability is also evaluated, as well as the linearity of the system. Finally, the MWP filter operation without resorting to off-chip optical amplification is considered, for investigating the possibility of further improving the system miniaturization.

A. Tuning of SiP MWP Filter Frequency and BW

For the narrowest BW tuning setting of the DFBR OF, corresponding to the traces of Fig. 4, and a detuning between the optical carrier and the passband center of 15 GHz, the measured squared magnitude of the S_{21} parameter from the VNA is displayed in Fig. 9(a). An out-of-band RF power rejection (OBPR) well above 40 dB over the considered frequency range of more than 60 GHz is observed. The measured −6 dB BW of 4.8 GHz well agrees with the DFBR filter BW, and the filter roll-off is larger than 7 dB/GHz over an excursion of more than 30 dB in its transition band. The results relative to the tuning of the integrated MWP filter central frequency with 7.5 GHz steps are also shown in Fig. 9(b). In the figure, the normalized filter response for the lowest frequency tuning at 7.5 GHz is taken as a reference, and all the other traces are displayed by bringing the high-frequency noise floor level to that of the reference trace. This allows clear comparison of the MWP filter performance in terms of OBPR as its central frequency is swept. The typical optimized reverse bias voltage of the modulator in the measurements is between 3.5 and 5 V, and the carrier-to-scanning sideband level at the PD input is adjusted through the VOS for maximized OBPR, while keeping fixed the overall received power at ∼ 6 dBm using an optical variable attenuator. This value, that is safely below the damage threshold of 10 dBm for the employed PD, corresponds to the minimum power available at the output of the OBPF
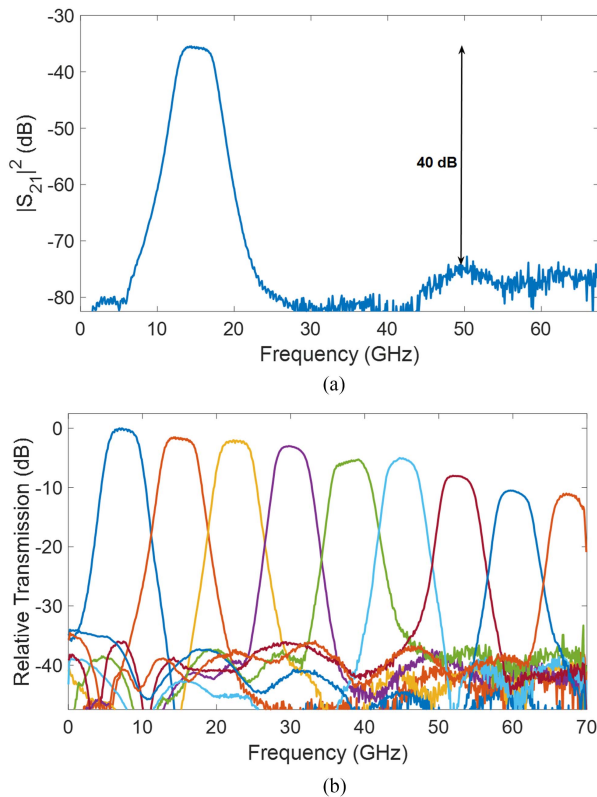
Fig. 9. (a) Measured power transmission of a 5 GHz-bandwidth SiP MWP filter for a laser carrier-to-DFBR filter detuning of 15 GHz. (b) Filter response for different tuning of the central frequency in the range $0 - 70$ GHz.
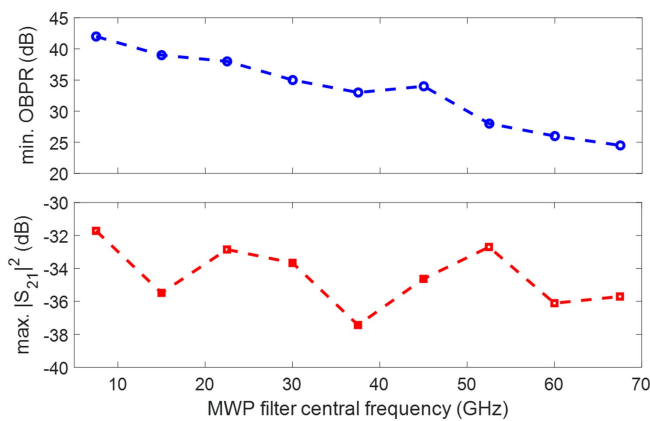

Fig. 10. Summary of the measured minimum full-span out-of-band power rejection (OBPR) and RF peak power transmission as a function of integrated microwave photonic filter central frequency corresponding to the noise-floor-normalized traces of Fig. 8(b).

following the EDFA for the maximum carrier-filter detuning of 67.5 GHz, although up to about 14 dBm was observed for the lowest frequency tuning settings.

The measured values for the minimum OBPR and maximum RF power transmission of the integrated MWP filter as a function of its central frequency are summarized in Fig. 10. The measurements indicate that a minimum OBPR of 35 dB is preserved over the full 70 GHz span when tuning the MWP filter central frequency up to 45 GHz. At larger detuning between the TLS

carrier and DFBR passband window the OBPR decrease is associated with an increased noise floor and is consistent with the measured roll-off in the modulator frequency response. The filter rejection is nevertheless about 25 dB for the maximum central frequency tuning of 67.5 GHz. Through proper optimization of the VOS and modulator bias, the variations of the measured $|S_{21}|^2$ peak values are confined to within less than 4 dB (neglecting the value at 37.5 GHz). By employing a laser source with larger output power or a second EDFA at the PIC input in conjunction with a high-power handling PD or an array of PDs [38], [39], larger values for the MWP filter peak transmission could be achieved. For the sake of simplicity, the integrated MWP filter tuning is here obtained by changing the TLS output wavelength, while keeping fixed the DFBR filter central wavelength. Alternatively, the LH structure could be employed to tune the MWP filter without changing its BW value at a fixed laser wavelength, as shown in Fig. 6. For all the measurements, the RF power delivered to the 70 GHz-BW probes contacting the PM is set to 0 dBm, corresponding to second-order sidebands from the PM that are about 35 dB lower than the relevant first-order sidebands. Since the modulator operates in almost linear regime at these levels, the same filter characteristics are obtained when reducing the RF power level at the probes to -10 dBm, for even larger second-order sideband suppression, at the expenses of slightly noisier signals at the PD output.

A similar filter tuning characterization is then repeated for the case in which the DFBR filter settings lead to the passband windows reported in in Fig. 5. For the case named *"BW tuning 1"*, leading to a -6 dB BW of about 7.5 GHz in the MWP bandpass filter power transmission, the tuning of the central frequency with 10 GHz steps between 10 and 60 GHz is shown in Fig. 11(a). For the DFBR setting named *"BW tuning 2"*, the MWP filter exhibits a typical passband width of about 10 GHz, with a tuning characterization reported in Fig. 11(b). It can be seen that for both the measurements, a large OBPR of more than 35 dB is attained over a tuning span of at least 40 GHz, with minimum rejection at the maximum detuning that is again larger than 25 dB. As shown in the trace of Fig. 5(a) for the case of largest detuning from the Bragg wavelength, a useful stopband portion on the lower-wavelength side of the passband of about 200 GHz is preserved. This suggests that, with an optimized modulator bandwidth, the tuning range of the integrated MWP filter could be further extended under any considered bandwidth configuration. Such a wide tuning operation would be hard to realize using for instance coupled MRRs as the filtering element, as the free-spectral-range of GHz-bandwidth MRRs-based filters is typically limited to few tens of GHz [40], [41], unless Vernier-based approaches are used [42]. However, the bandwidth reconfigurability in coupled MRRs OFs requires acting on the inter-rings coupling coefficients through tunable elements, which further complicates the filter design and control circuitry.

B. RF Gain and Linearity Characterization

By acting on the VOS separating the input laser carrier after the optical input port of the PIC, the transmission characteristics
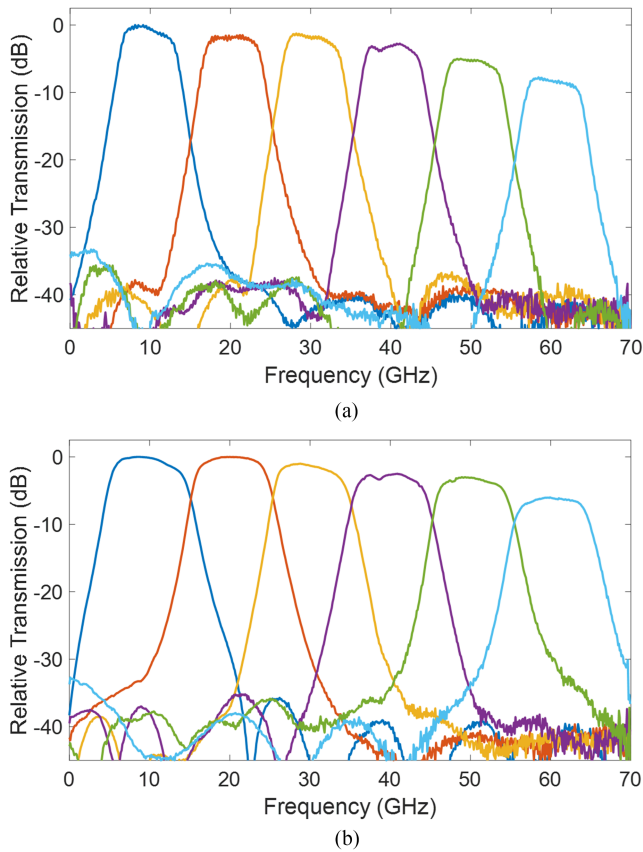
Fig. 11. Tuning characteristics of the integrated microwave photonic filter for typical bandwidth values of about (a) 7.5 and (b) 10 GHz.
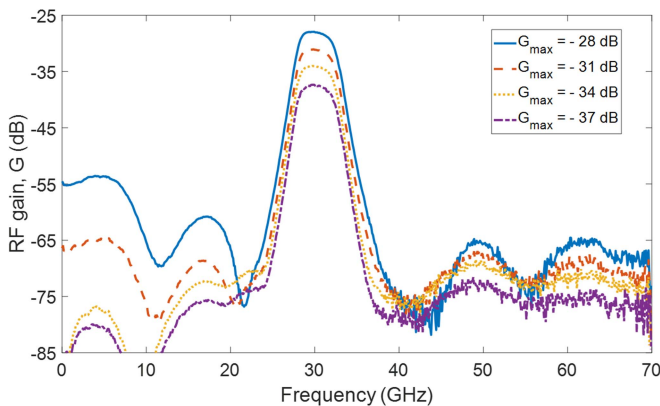

Fig. 12. Different spectral RF gain ($|S_{21}|^2$) of the integrated microwave photonic filter centered at 30 GHz with fine control of the variable optical splitter.

of the MWP filter can be finely adjusted. This feature might turn useful for shaping the filter performance for a desired target application. This is shown for the case of a passband centered at 30 GHz in the traces of Fig. 12, where the squared modulus of the S_{21} parameter from the VNA (i.e., the RF gain of the system, assumimg the same input/output impedance [43]) is measured for different levels of the carrier-to-scanning sideband power ratio at the PD input, for a fixed overall optical power of about 6 dBm. For the case in which a maximum RF gain, G_{max}, of -28 dB is obtained, a poor filter rejection at frequencies

below about 20 GHz is observed. This limits the full-span OBPR to about 26 dB. Nevertheless, between 20 and 70 GHz the OBPR stays well above 35 dB. As the value of G_{max} decreases, however, the suppression of spurious components in the low-frequency region sensibly improves. An optimal OBPR of 37 dB over the full 70 GHz span (as in the 30 GHz-centered trace of Fig. 9) is obtained when $G_{max} = -34$ dB. The limited OBPR behavior at high RF gain is ascribed to the improved modulation efficiency of the equivalent MZI structure that is experienced by the residual optical components falling within the DFBR OF stopband. Since the modulator response is maximum between DC and about 20 GHz, the OSBR degradation is correspondingly larger in that range. On the other hand, in the high portion of the scanned spectrum, the measurement floor is mainly set by the different noise sources in the system. By reducing the strength of the low-frequency noisy terrms originated by the beating between the optical carrier and spurious sideband components acting on the MZI unbalance through the VOS, it is thus possible to extend the high OBPR frequency range at the only expense of a moderate RF gain reduction. This feature can also be exploited for optimizing the selectivity and/or RF gain of the integrated MWP over specific operating frequency bands.

As mentioned, higher RF gains can be in principle attained by increasing the optical power coupled into the chip in conjunction with a large-power-handling PD as well as by optimizing the modulator design for reducing its half-wave voltage. A larger optical power at the PIC output would also be beneficial for decreasing the noise contribution from the following EDFA. Improving the RF gain, along with using a low-RIN laser source and low-noise EDFAs, would also contribute to reduce the noise figure of the proposed MWP filter, as requested for practical system applications. However, the SiP PIC input power cannot be indefinitely increased without triggering two-photon absorption (TPA) and subsequent free-carrier absorption effects in the silicon waveguides. To reduce the TPA threshold, the DFBR OF and circuit connections can be designed using rib waveguides with larger modal area than the current strip-waveguide implementation [44].

The spurious-free dynamic range (SFDR) of the SiP MWP filter is then assessed in a standard two-tone measurement. The DFBR filter-to-optical carrier detuning is set at 11 GHz, and two CW RF signals at ±100 MHz from the filter central frequency have been simultaneously applied with the same power to the SiP PM. By varying the power of the two RF tones and monitoring the PD output signal on an electrical spectrum analyzer (ESA), the amplitude of the third-order intermodulation distortion (IMD3) term at 10.7 GHz is recorded, along with that of the original tone at 11.1 GHz. The results of the measurement are reported in Fig. 13, indicating a SFDR of nearly 96 dB·$Hz^{2/3}$. This value is in accordance with those previously reported for SiP modulators, for which the system linearity is mainly limited by the physics of the plasma dispersion effect in the carrier-depletion based device [45]. The SFDR could be for instance improved by implementing the PIC using the lithium-niobate-on-insulator (LNOI) technological platform, where linear Pockels-based EO modulation mechanism is available for realizing high-speed efficient phase modulators [46], and
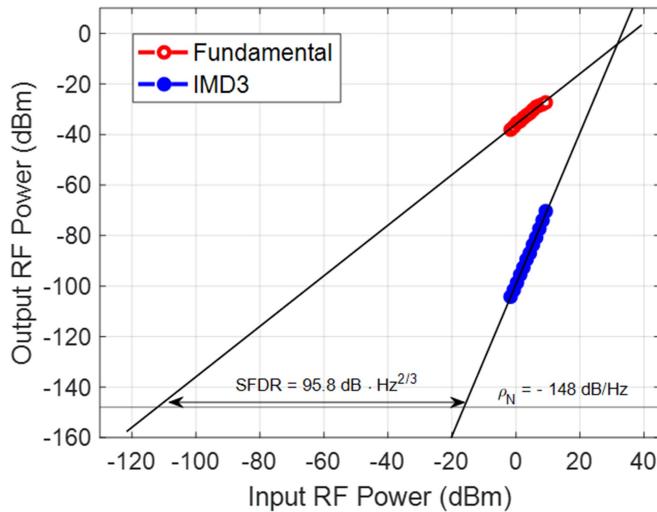
Fig. 13.   Spurious-free dynamic range measurements results.

Fig. 14.   Measured squared magnitude of S_{21} parameter for the integrated microwave photonic filter centered at 30 GHz by directly connecting the PIC output to the PD and using RF amplification. Two different settings of the variable optical splitter (VOS) are reported, and the noise floor of the vector network analyzer instrument when the photodiode is disconnected by its input port is also displayed.

waveguide Bragg grating filters have also been recently demonstrated [47], [48].

C. Integrated MWP Filter Operation Without Optical Amplification

Finally, the possibility of improving the integration level of the SiP MWP bandpass filter is evaluated. As shown in the mask layout of the fabricated PIC reported in Fig. 2, a Ge PD has also been inserted in the circuit. However, the high level of electromagnetic crosstalk between the transmitting and receiving equipment in the setup and the limited optical power available at the SiP PD prevented meaningful measurements using on-chip photodetection. Nevertheless, the circuit operation for the case in which the EDFA at the PIC output is eliminated and the optical output of the circuit is directly connected to an external 50 GHz-BW PD followed by an RF amplification stage has been investigated. A booster amplifier, operating in the frequency range between 18 and 46 GHz, with a small signal gain of 35 dB, and a typical noise figure of 8 dB has been used.

The measured squared magnitude of the S_{21} parameter for a passband tuned at about 30 GHz are shown in Fig. 14 for two different settings of the VOS. The margin for taking advantage of the discussed trade-off between RF gain and filter rejection is now sensibly reduced. For the case with the highest RF gain of -39 dB, named *"measure 1"* in the figure, an OBPR of 25 dB is obtained, which improves to 28 dB for the case named *"measure 2"*, for which the RF gain is reduced to -42 dB. The considered OBPR values are calculated in the frequency span between 17.5 and about 38 GHz. Above the high-frequency edge of the filter, indeed, the floor level of the measured traces sensibly rises due to the residual RF crosstalk that is captured from the VNA input port. This is confirmed by the measured values of $|S_{21}|^2$ for the case in which the PD is disconnected from the VNA input port. Due to the larger crosstalk with increased radiation frequency, the disturbance gets higher than the system noise floor above about 40 GHz. Apart for this RF interference issue, the results generally indicate an overall reduced performance with
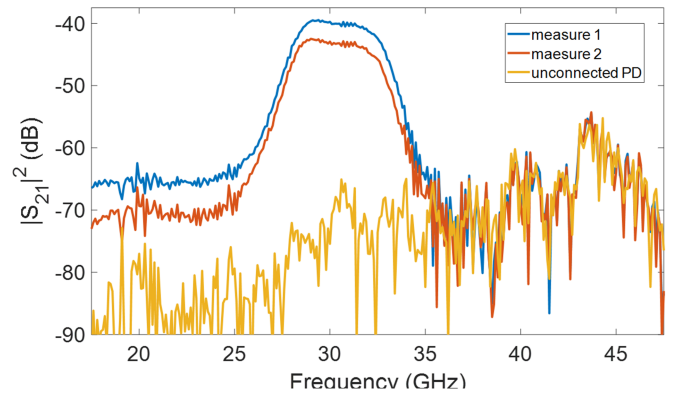
respect to the case of using an EDFA after the PIC. A possible way for approaching the performance obtained with the optically amplified signals through the external EDFA would be by using low-noise RF amplifiers specifically designed for low-power signals [49], [50], or by means of on-chip amplification using hybrid integration techniques [51], [52]. A combination of both approaches could also be employed, in conjunction with design strategies for improving the isolation between the input and output RF ports of the circuit, for the development of monolithic full on-chip integrated MWP filter functionality.

V. CONCLUSION

The results of an integrated microwave photonic (MWP) filter, with wide tunability of the center frequency and of the flat-top passband width has been presented. High levels of filter rejection and roll-off as well as preserved passband shape under frequency tuning over 70 GHz range and bandwidth variation from about 5 to 10 GHz have been observed. The photonic integrated circuit (PIC) has been realized in CMOS-compatible silicon on insulator technology using standard lithographic process. The circuit accepts at its input ports an optical carrier and the RF signal to be processed and deliver the optical output for down-conversion to the RF domain in a high-speed external photodiode (PD). With respect to previously reported integrated reconfigurable MWP bandpass filter realizations, the proposed circuit represents a fair improvement of the integration degree of the RF filtering functionality in an ultra-compact layout of about 1.5 mm^2, while guaranteeing high-level performance. Possibility of further improving the miniaturization level toward monolithic on-chip operation has also been investigated and discussed. The device exploits the bandwidth reconfigurability of a distributed feedback resonator (DFBR) optical filter realized in a waveguide Bragg grating structure which is sampled by the sideband of a 30 GHz-bandwidth phase modulator (PM). Additional tunable control for the carrier and sideband relative amplitude is employed for fine optimization of the operation. The integrated MWP filter features can be tailored for targeting

different bandwidth values by adjusting the parameters of the DFBR, that can be designed to provide a bandpass transfer function as narrow as 1 GHz [29], [53] or below, suitable for instance for channelizing operation in high-capacity next generation mobile networks. At the same time, the operating frequency range can be further extended by optimizing the silicon photonics PM bandwidth [54], [55]. The presented results illustrate the potentiality of this approach for realizing ultra-compact and cost-effective RF signal processors for broadband signals in several emerging applications in the fields of millimeter-wave wireless communications and sensing.

ACKNOWLEDGMENT

REFERENCES

[1] E. J. Norberg, R. S. Guzzon, J. S. Parker, L. A. Johansson, and L. A. Coldren, "Programmable photonic microwave filters monolithically integrated in InP–InGaAsP," *J. Lightw. Technol.*, vol. 29, no. 11, pp. 1611–1619, Jun. 2011.

[2] X. Xue et al., "Programmable single-bandpass photonic RF filter based on Kerr comb from a microring," *J. Lightw. Technol.*, vol. 32, no. 20, pp. 3557–3565, Oct. 2014.

[3] J. S. Fandiño, P. Muñoz, D. Doménech, and J. Capmany, "A monolithic integrated photonic microwave filter," *Nature Photon.*, vol. 11, no. 2, pp. 124–129, 2017.

[4] H. Qiu et al., "A continuously tunable sub-gigahertz microwave photonic bandpass filter based on an ultra-high-Q silicon microring resonator," *J. Lightw. Technol.*, vol. 36, no. 19, pp. 4312–4318, Oct. 2018.

[5] W. Zhang and J. Yao, "On-chip silicon photonic integrated frequency-tunable bandpass microwave photonic filter," *Opt. Lett.*, vol. 43, no. 15, pp. 3622–3625, 2018.

[6] E. A. Kittlaus, P. Kharel, N. T. Otterstrom, Z. Wang, and P. T. Rakich, "RF-photonic filters via on-chip photonic–phononic emit–receive operations," *J. Lightw. Technol.*, vol. 36, no. 13, pp. 2803–2809, Jul. 2018.

[7] X. Xu et al., "Advanced adaptive photonic RF filters with 80 taps based on an integrated optical micro-comb source," *J. Lightw. Technol.*, vol. 37, no. 4, pp. 1288–1295, Feb. 2019.

[8] Y. Xie et al., "System-level performance of chip-based Brillouin microwave photonic bandpass filters," *J. Lightw. Technol.*, vol. 37, no. 20, pp. 5246–5258, Oct. 2019.

[9] Z. Zhu, Y. Liu, M. Merklein, O. Daulay, D. Marpaung, and B. J. Eggleton, "Positive link gain microwave photonic bandpass filter using Si$_3$N$_4$-ring-enabled sideband filtering and carrier suppression," *Opt. Exp.*, vol. 27, no. 22, pp. 31727–31740, 2019.

[10] P. Zheng et al., "Manipulation microwave photonic filter response of single microring by using optical frequency combs," *Opt. Commun.*, vol. 459, 2020, Art. no. 125069.

[11] Y. Tao et al., "Hybrid-integrated high-performance microwave photonic filter with switchable response," *Photon. Res.*, vol. 9, no. 8, pp. 1569–1580, Aug. 2021.

[12] O. Daulay et al., "Ultrahigh dynamic range and low noise figure programmable integrated microwave photonic filter," 2022. [Online]. Available: https://arxiv.org/abs/2203.04724

[13] J. Capmany and P. Muñoz, "Integrated microwave photonics for radio access networks," *J. Lightw. Technol.*, vol. 32, no. 16, pp. 2849–2861, Aug. 2014.

[14] B. Batagelj, J. Capmany, and E. G. Udvary, "5th-generation mobile access networks assisted by integrated microwave photonics," in *Proc. Int. Workshop Fiber Opt. Access Netw.*, 2019, pp. 1–6.

[15] D. Marpaung, J. Yao, and J. Capmany, "Integrated microwave photonics," *Nature Photon.*, vol. 13, no. 2, pp. 80–90, 2019.

[16] World Radiocommunication Conference, 20ll5. [Online]. Available: http://www.itu.int/en/ITUR/conferences/wrc/2015/

[17] S. Tripathi, N. V. Sabu, A. K. Gupta, and H. S. Dhillon, "Millimeter-wave and terahertz spectrum for 6G wireless," in *6G Mobile Wireless Networks*. Berlin, Germany: Springer, 2021, pp. 83–121.

[18] C. Riva, C. Capsoni, L. Luini, M. Luccini, R. Nebuloni, and A. Martellucci, "The challenge of using the W band in satellite communication," *Int. J. Satell. Commun. Netw.*, vol. 32, no. 3, pp. 187–200, 2014.

[19] R. K. Garg, S. Singhal, and R. Tomar, "A CPW fed clown-shaped super wideband antenna," *Prog. Electromagn. Res. Lett.*, vol. 99, pp. 159–168, 2021.

[20] S. Dey, M. S. Arefin, and N. C. Karmakar, "Design and experimental analysis of a novel compact and flexible super wide band antenna for 5G," *IEEE Access*, vol. 9, pp. 46698–46708, 2021.

[21] M. Abdelfattah, D. Psychogiou, Z. Yang, and D. Peroulis, "V-band frequency reconfigurable cavity-based bandpass filters," in *Proc. IEEE/ACES Int. Conf. Wireless Inf. Tech. Syst. Appl. Comput. Electromagn.*, 2016, pp. 1–2.

[22] Z. Ge, L. Chen, R. Gomez-Garcia, and X. Zhu, "Millimeter-wave wideband bandpass filter in CMOS technology using a two-layered highpass-type approach with embedded upper stopband," *IEEE Trans. Circuits Syst. II Exp. Briefs*, vol. 68, no. 5, pp. 1586–1590, May 2021.

[23] B. Chen, S. K. Thapa, A. Barakat, and R. K. Pokharel, "A W-band compact substrate integrated waveguide bandpass filter with defected ground structure in CMOS technology," *IEEE Trans. Circuits Syst. II Exp. Briefs*, vol. 69, no. 3, pp. 889–893, Mar. 2022.

[24] J. E. Román, M. Y. Frankel, and R. D. Esman, "Spectral characterization of fiber gratings with high resolution," *Opt. Lett.*, vol. 23, no. 12, pp. 939–941, 1998.

[25] R. Hernández, A. Loayssa, and D. Benito, "Optical vector network analysis based on single-sideband modulation," *Opt. Eng.*, vol. 43, no. 10, pp. 2418–2421, 2004.

[26] C. Porzi, F. Falconi, M. Sorel, and A. Bogoni, "Broadband and high-capacity silicon photonics single-sideband modulator," *J. Lightw. Technol.*, vol. 40, no. 2, pp. 538–546, Jan. 2022.

[27] L. Ulrich et al., "High rejection photonic RF filter using a thulium doped crystal," in *Proc. IEEE Int. Top. Meet. Microw. Photon.*, 2021, pp. 1–4.

[28] Compoundtek. [Online]. Available: https://compoundtek.com/

[29] C. Porzi, G. J. Sharp, M. Sorel, and A. Bogoni, "Silicon photonics high-order distributed feedback resonators filters," *IEEE J. Quantum Electron.*, vol. 56, no. 1, pp. 1–9, Feb. 2020.

[30] V. Wong, J. Ferrera, J. Damask, T. Murphy, H. I. Smith, and H. Haus, "Distributed Bragg grating integrated-optical filters: Synthesis and fabrication," *J. Vac. Sci. Technol. B*, vol. 13, no. 6, pp. 2859–2864, 1995.

[31] C. Porzi, G. Serafino, P. Velha, P. Ghelfi, and A. Bogoni, "Integrated SOI high-order phase-shifted Bragg grating for microwave photonics signal processing," *J. Lightw. Technol.*, vol. 35, no. 20, pp. 4479–4487, Oct. 2017.

[32] C. Porzi, G. J. Sharp, M. Sorel, and A. Bogoni, "High-contrast, flat-top, silicon-photonics passband optical filters with high-order phase-shifted Bragg gratings," in *Proc. 44th Eur. Conf. Opt. Commun.*, Rome, 2018, Paper Mo3C.5.

[33] L. A. Coldren, S. W. Corzine, and M. L. Mashanovitch, *Diode Lasers and Photonic Integrated Circuits*. Hoboken, NJ, USA: Wiley, 2012.

[34] L. Chrostowski and M. Hochberg, *Silicon Photonics Design: From Devices to Systems*. Cambridge, U.K.: Cambridge Univ. Press, 2015.

[35] F. Falconi, C. Porzi, G. J. Sharp, M. Sorel, and A. Bogoni, "Widely tunable silicon photonics narrow-linewidth passband filter based on phase-shifted waveguide Bragg grating," in *IEEE Int. Top. Meet. Microw. Photon.*, Tolouse, 2018, pp. 1–4.

[36] K. Chen, F. Duan, and Y. Yu, "High-performance thermo-optic tunable grating filters based on laterally supported suspended silicon ridge waveguide," *Opt. Exp.*, vol. 26, no. 15, pp. 19479–19488, 2018.

[37] D. Mu et al., "A four-channel DWDM tunable add/drop demultiplexer based on silicon waveguide Bragg gratings," *IEEE Photon. J.*, vol. 11, no. 1, pp. 1–8, Feb. 2019.

[38] K. Sun and A. Beling, "High-speed photodetectors for microwave photonics," *Appl. Sci.*, vol. 9, no. 4, pp. 623–638, 2019.

[39] K. Sun, J. Gao, R. Costanzo, T.-C. Tzu, S. M. Bowers, and A. Beling, "Germanium photodiode arrays on silicon-on-insulator with on-chip bias circuit," *IEEE Photon. Technol. Lett.*, vol. 33, no. 16, pp. 832–835, Aug. 2021.

[40] P. Dong et al., "GHz-bandwidth optical filters based on high-order silicon ring resonators," *Opt. Exp.*, vol. 18, no. 23, pp. 23784–23789, 2010.

[41] Z. Geng et al., "Photonic integrated circuit implementation of a sub-GHz-selectivity frequency comb filter for optical clock multiplication," *Opt. Exp.*, vol. 25, no. 22, pp. 27635–27645, 2017.

[42] J. C. Mak, T. Xue, Z. Yong, and J. K. Poon, "Wavelength tunable matched-pair Vernier multi-ring filters using derivative-free optimization algorithms," *IEEE J. Sel. Top. Quantum Electron.*, vol. 26, no. 5, pp. 1–12, Sep./Oct. 2020.

[43] V. J. Urick, K. J. Williams, and J. D. McKinney, *Fundamentals of Microwave Photonics*. Hoboken, NJ, USA: Wiley, 2015.

[44] J. Bass, B. Brea, H. Tran, W. Du, R. Soref, and S.-Q. Yu, "The effect of two-photon absorption on the dynamic range of integrated microwave photonics links," in *Silicon Photonics XV*, vol. 11285. SPIE, 2020, pp. 216–223.

[45] X. Luo et al., "Slope efficiency and spurious-free dynamic range of silicon Mach-Zehnder modulator upon carrier depletion and injection effects," *Opt. Exp.*, vol. 21, no. 14, pp. 16570–16577, 2013.

[46] T. Ren et al., "An integrated low-voltage broadband lithium niobate phase modulator," *IEEE Photon. Technol. Lett.*, vol. 31, no. 11, pp. 889–892, Jun. 2019.

[47] K. Abdelsalam et al., "Tunable dual-channel ultra-narrowband Bragg grating filter on thin-film lithium niobate," *Opt. Lett.*, vol. 46, no. 11, pp. 2730–2733, 2021.

[48] A. Prencipe, M. A. Baghban, and K. Gallo, "Tunable ultranarrowband grating filters in thin-film lithium niobate," *ACS Photon.*, vol. 8, no. 10, pp. 2923–2930, 2021.

[49] H. P. E. Morath, P. V. Testa, J. Wagner, and F. Ellinger, "A 3.6 mW 60 GHz low-noise amplifier with 0.6 ns settling time for duty-cycled receivers," *IEEE Microw. Wirel. Compon. Lett.*, vol. 31, no. 8, pp. 977–980, Aug. 2021.

[50] D. Pan, Z. Duan, S. Chakraborty, L. Sun, and P. Gui, "A 60-GHz CMOS double-neutralized LNA technology with 6.3-dB NF and dBm P_{-1dB}," *IEEE Microw. Wirel. Compon. Lett.*, vol. 29, no. 7, pp. 489–491, Jul. 2019.

[51] M. L. Davenport, S. Skendžić, N. Volet, J. C. Hulme, M. J. R. Heck, and J. E. Bowers, "Heterogeneous silicon/III–V semiconductor optical amplifiers," *IEEE J. Sel. Top. Quantum Electron.*, vol. 22, no. 6, pp. 78–88, Nov./Dec. 2016.

[52] K. V. Gasse, R. Wang, and G. Roelkens, "27 dB gain III-V-on-silicon semiconductor optical amplifier with >17 dBm output power," *Opt. Exp.*, vol. 27, no. 1, pp. 293–302, 2019.

[53] C. Porzi, M. Reza, M. Sorel, and A. Bogoni, "Frequency and bandwidth tunable integrated microwave photonic bandpass filter," in *Proc. Int. Workshop Fiber Opt. Access Netw.*, Oct. 2022, pp. 1–5.

[54] H. Zwickel et al., "Verified equivalent-circuit model for slot-waveguide modulators," *Opt. Exp.*, vol. 28, no. 9, pp. 12951–12976, 2020.

[55] H. Zhang et al., "800 Gbit/s transmission over 1 km single-mode fiber using a four-channel silicon photonic transmitter," *Photon. Res.*, vol. 8, no. 11, pp. 1776–1782, 2020.

Claudio Porzi received the Laurea degree in electronics engineering from the "La Sapienza" University of Rome, Rome, Italy, in 2000, and the Ph.D. degree in telecommunications from Scuola Superiore Sant'Anna (SSSA), Pisa, Italy, in 2005. He is currently an Assistant Professor with SSSA, working on the design and characterization of photonic integrated circuits for telecom/datacom and microwave photonics applications. He has coauthored more than 150 research articles published in peer-reviewed journals or presented at major international conferences.

Manuel Reza received the Ph.D. degree in electronic and electrical engineering from the University of Glasgow, Glasgow, U.K., where he was involved with the design of active semiconductor devices for mid-infrared sensing applications. He is currently a Research Assistant with the Sant'Anna School of Advanced Studies of Pisa, Italy. He is currently involved with projects related to the design of photonic integrated circuits for microwave applications, in particular optical and optically-assisted beamforming, photonic RF scanners, coherent MIMO radars for ground, and space-borne applications.

Paolo Ghelfi received the M.Sc. degree in electronic engineering in 2000. Since 2001, he has been with PNT Laboratory, CNIT, Pisa, Italy, where he is currently the Head of Research Area. He has authored or coauthored more than 40 papers on international journals, more than 110 papers on international conferences, more than 20 patents, and two book chapters. His research interests include microwave photonics, with strong experience also in the fields of high bit rate fiber-optic transmission systems, all-optical signal processing, and reconfigurable networks.

Marc Sorel (Senior Member, IEEE) received the Laurea degree (cum laude) in electrical and electronics engineering and the Ph.D. degree in electronics and computer science from the Università di Pavia, Pavia, Italy, in 1995 and 1999, respectively. He joined the Optoelectronics Research Group with the University of Glasgow, Glasgow, U.K., in 1998, with a Rotary Foundation Fellowship and was the recipient of personal MarieCurie Fellowship in 1999. He was appointed a Professor of Optoelectronics in 2015. He was involved with the field of integrated photonic devices for more than 20 years. He has authored or coauthored more than 200 articles in peer-reviewed journals and he has made numerous presentations at major national and international conferences. He was with the scientific committees of several international conferences, such as ECIO, ECOC, Photonics North, CLEO Europe, and the IEEE Photonics Annual Meeting. His research interests include silicon photonics, semiconductor lasers, photonic integration, and mid-IR optoelectronic devices for sensing.

Antonella Bogoni (Member, IEEE) is currently a Full Professor with the Sant'Anna School of Advanced Studies, Pisa, Italy, and the Director of the PNT Laboratory, CNIT, Pisa, Italy. Moreover, she is leading the design of specific photonic integrated circuits for implementing on-chip the proposed solutions. She has been scientific responsible for 48 grants 27 as PI or coordinator. She has authored or coauthored 56 patents, eight books and chapters, and more than 160 papers on the main scientific international journals 22 invited contributions. Her research interests include photonics technologies for optical fiber networks for ultrafast optical signal processing and microwave systems, especially for 5G, radars, and space applications. She has more than 300 contributions in the main photonics and radar international conferences, winning nine Best Paper awards, with more than 90 invited contributions. In 2014 and 2020, she was the Topical Editor of Optics Letters and Guest editors of nine special issues on international journals. She is the Chair of conferences and workshops, including the General Chair of MWP 2021 and Photonics in Switching 2014, Program Chair of ECOC 2018.